Influence of materials' optical response on actuation dynamics by Casimir forces

Sedighi Ghozotkhar, Mehdi; Broer, W. H.; Van der Veeke, S.; Svetovoy, V. B.; Palasantzas, G.

Published in:
Journal of Physics-Condensed Matter

DOI:
10.1088/0953-8984/27/21/214014

IOP Publishing Journal of Physics: Condensed Matter
J. Phys.: Condens. Matter **27** (2015) 214014 (6pp) doi:10.1088/0953-8984/27/21/214014

Influence of materials' optical response on actuation dynamics by Casimir forces

M Sedighi[1], W H Broer[1], S Van der Veeke[1], V B Svetovoy[2] and G Palasantzas[1]

[1] Zernike Institute for Advanced Materials, University of Groningen, Nijenborgh 4, 9747 AG Groningen, The Netherlands
[2] MESA+ Institute for Nanotechnology, University of Twente, PO 217, 7500 AE Enschede, The Netherlands

E-mail: g.palasantzas@rug.nl

Received 15 September 2014, revised 30 October 2014
Accepted for publication 11 November 2014
Published 12 May 2015

Abstract

The dependence of the Casimir force on the frequency-dependent dielectric functions of interacting materials makes it possible to tailor the actuation dynamics of microactuators. The Casimir force is largest for metallic interacting systems due to the high absorption of conduction electrons in the far-infrared range. For less conductive systems, such as phase change materials or conductive silicon carbide, the reduced force offers the advantage of increased stable operation of MEMS devices against pull-in instabilities that lead to unwanted stiction. Bifurcation analysis with phase portraits has been used to compare the sensitivity of a model actuator when the optical properties are altered.

Keywords: Casimir force, optical properties, MEMS

(Some figures may appear in colour only in the online journal)

1. Introduction

The application of modern microelectromecanical systems (MEMS) is becoming increasingly important in science and technology, which simultaneously reveals the significant role of the Casimir force for the analysis and design of microsystems [1]. The Casimir force was predicted by Casimir in 1948 [2] as a mutual attraction between two perfectly reflecting parallel plates separated by a small vacuum gap, due to quantum fluctuations of the electromagnetic (EM) field [1–13]. Later on, Lifshitz [3] considered the more general case of real dielectric plates by exploiting the fluctuation–dissipation theorem, which relates the dissipative properties of the plates (optical absorption by many microscopic dipoles) and EM fluctuations. The Lifshitz theory predicts the attractive force between the two parallel plates of arbitrary materials, and covers both the van der Waals (short-range) and Casimir (long-range) asymptotic regimes [1, 3].

While the relation between the EM vacuum fluctuations and the Casimir force has some fundamental significance, the dependence of the Casimir force on material optical properties is an outstanding outcome of the Lifshitz theory [3]. It allows one to tailor the force by a suitable choice of the interacting materials [6–14], which consequently opens a new window of opportunity for MEMS engineering. These devices have surface areas large enough but gaps small enough for the Casimir force to pull components together, which leads to permanent adhesion or stiction. This malfunction is very important for the dynamical stability of MEMS: not only as a problem [1, 4], but also as a means to utilize the irreversible adhesion of moving parts to add new functionalities to MEMS architectures [1].

So far, a wide range of materials with realistic optical properties have been used [5–13] to measure and calculate the Casimir force. However, a comprehensive study to compare the effects of different materials—with gradually variable conduction properties—on MEMS actuation has not been performed. Here we analyse three conductive materials with very different optical properties to understand the influence of these properties on the stability of MEMS devices.

2. Optical response and Casimir force calculations

The materials analysed in this paper include metallic Au films of which the optical properties have been measured in a wide range of frequencies for different preparation

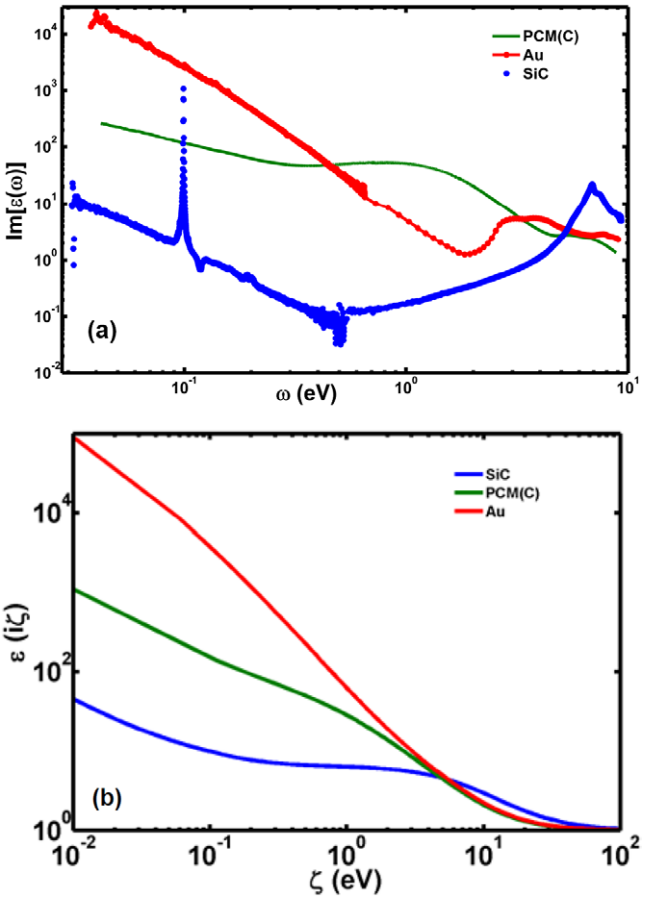

Figure 1. (*a*) Imaginary part $\varepsilon''(\omega)$ of the frequency-dependent dielectric function measured with ellipsometry for Au, crystalline AIST (PCM), and conductive SiC. Here we use the data for Au from the sample 3 in [11] unless it is specified otherwise. (*b*) The corresponding dielectric functions $\varepsilon(i\zeta)$ from (*a*) calculated using the Drude model.

conditions [11]. Gold is widely used for Casimir force measurements. As a representative of a narrow bandgap semiconductor, we consider the phase change material (PCM) AIST $Ag_5In_5Sb_{60}Te_{30}$ which has an amorphous (A) phase (with a band gap of $E_g = 0.63$ eV), whereas the crystalline (C) phase is highly conductive (with a band gap of $E_g = 0.18$ eV) [15]. Optical properties of AIST were measured and analysed in [8, 9]. Finally, as a wide bandgap material we consider silicon carbide (SiC) which becomes conductive due to nitrogen doping. This material has a prominent phonon-polariton peak. (See [16] for measurements and a description of the properties of SiC.) All three materials were optically characterized with the same equipment (J A Woollam Co., Inc. ellipsometers VUV-VASE (0.5–9.34 eV) and IR-VASE (0.03–0.5 eV)). The imaginary parts of the dielectric functions of all three materials are shown in figure 1(*a*).

PCM and SiC not only have specific applications in different fields, but they represent exciting new possibilities for applications involving the Casimir force [8, 9, 16]. Indeed, PCMs are known for their application in data storage (CD, DVD and Blu-ray disks) [15]. Moreover, they represent potential new ideas to be implemented in MEMS actuators [9, 17], because changing the material phase from amorphous to crystalline (by means of e.g. heating or a laser pulse) leads to a Casimir force contrast of up to 25% [8, 9]. On the other hand, SiC is a candidate to replace silicon for the operation of MEMS sensors under severe conditions in automotive and space applications etc [19, 20].

Before modeling the actuation dynamics we will first illustrate the influence of the optical properties of different materials on the Casimir force via Lifshitz theory calculations. In order to avoid parallelism problems, which are considerable at nanoscale separations, in practice the plate-sphere geometry is typically used for force measurements [8–12]. Within the proximity force approximation (PFA), the Casimir force at separations $z \ll R$, where R is the sphere's radius, is given by

$$F^{\mathrm{ps}}(z) = \frac{\hbar c R}{16\pi z^3} \sum_{\nu} \int_0^1 \mathrm{d}t \int_0^{\infty} \mathrm{d}x x^2 \ln\left(1 - r_1^{\nu} r_2^{\nu} \mathrm{e}^{-x}\right). \tag{1}$$

This is valid for zero temperature calculations or for short separations ($z < 300$ nm) at room temperature (where thermal fluctuations have negligible contribution since the corresponding thermal wavelength $\lambda_T = 7.6\,\mu$m is much larger). Here $\hbar$ is the Planck constant and c is the speed of light. The integration variables are defined as $x = 2k_0 z$ and $tx = \zeta/\zeta_{\mathrm{ch}}$, and $\zeta_{\mathrm{ch}} = c/2z$ is the characteristic imaginary frequency. The indices $\nu = s$ (TE mode) and p (TM mode) denote the two polarizations, and $r_{1,2}^{\nu}$ are the Fresnel reflection coefficients for bodies 1 and 2. The wavenumbers perpendicular to the plates are in the ith material $k_i = \sqrt{\varepsilon_i(i\zeta)\left(\zeta^2/c^2\right) + q^2}$ and in a vacuum (or air) $k_0 = \sqrt{\left(\zeta^2/c^2\right) + q^2}$ with q being the wavenumber along the plates. The reflection coefficients $r_{1,2}^{\nu}$ for homogeneous materials are the Fresnel coefficients, defined as

$$r_i^s = \frac{1 - \sqrt{1 + t^2\left(\varepsilon_i(i\zeta) - 1\right)}}{1 + \sqrt{1 + t^2\left(\varepsilon_i(i\zeta) - 1\right)}},$$
$$r_i^p = \frac{\varepsilon_i - \sqrt{1 + t^2\left(\varepsilon_i(i\zeta) - 1\right)}}{\varepsilon_i + \sqrt{1 + t^2\left(\varepsilon_i(i\zeta) - 1\right)}}. \tag{2}$$

Finally, an important ingredient for Casimir force calculations is the dielectric function at imaginary frequencies $\varepsilon(i\zeta)$. This function is defined in terms of the measurable dielectric function at real frequencies by the Kramers–Kronig relation

$$\varepsilon(i\zeta) = 1 + \frac{2}{\pi} \int_0^{\infty} \frac{\omega \varepsilon''(\omega)}{\omega^2 + \zeta^2} \mathrm{d}\omega \tag{3}$$

In practice, however, the experimental data for the imaginary part $\varepsilon''(\omega)$ of the dielectric function $\varepsilon(\omega)$ cover only a limited frequency range, say $\omega_1 < \omega < \omega_2$ (figure 1(*a*)). For conductive materials that show significant absorption due to charge carriers in the infrared range, the dielectric function at low optical frequencies is described by the Drude model

$$\varepsilon(\omega)_{\mathrm{D}} = \varepsilon_{\mathrm{o}} - \frac{\omega_{\mathrm{p}}^2}{\omega(\omega + i\omega_\tau)}. \tag{4}$$

This model is often used for extrapolating in the low optical frequency regime $0 < \omega < \omega_1$ ($= 0.03$ eV). In equation (4) ω_p is the plasma frequency, ω_τ is the relaxation frequency, and the ratio ω_p^2/ω_τ is indicative of the material's static conductivity (at $\omega \to 0$) [8, 9, 11, 12, 16]. In the high optical frequency range, $\omega > \omega_2$, which is significant only at separations smaller than 10 nm, the permittivity is extrapolated as an inverse power law: $\varepsilon''(\omega) \sim 1/\omega^3$ [8, 9, 11, 12, 16]. Therefore, for frequencies $\omega < \omega_1$ and $\omega > \omega_2$, $\varepsilon''(\omega)$ is extrapolated as [16]

$$\omega < \omega_1\ (= 0.03\ \text{eV}): \qquad \varepsilon''(\omega) = \frac{\omega_p^2 \omega_\tau}{\omega\left(\omega^2 + \omega_\tau^2\right)},$$
$$\omega > \omega_2\ (= 9.34\ \text{eV}): \qquad \varepsilon''(\omega) = \frac{A}{\omega^3}. \tag{5}$$

Using the Drude model, one obtains for $\varepsilon(i\zeta)$ the convenient form

$$\varepsilon(i\zeta)_D = 1 + \frac{2}{\pi}\int_{\omega_1}^{\omega_2} \frac{\omega \varepsilon''_{exp}(\omega)}{\omega^2 + \zeta^2} d\omega + \Delta_L\varepsilon(i\zeta) + \Delta_H\varepsilon(i\zeta), \tag{6}$$

with

$$\Delta_H\varepsilon(i\zeta) = \frac{2}{\pi}\int_{\omega_2}^{\infty} \frac{\omega\varepsilon''(\omega)}{\omega^2+\zeta^2} d\omega = \frac{2\omega_2^3\varepsilon''(\omega_2)}{\pi\zeta^2}\left[\frac{1}{\omega_2} - \frac{\frac{\pi}{2} - \arctan(\omega_2/\zeta)}{\zeta}\right] \tag{7}$$

$$\Delta_L\varepsilon(i\zeta) = \frac{2}{\pi}\int_{0}^{\omega_1} \frac{\omega\varepsilon''(\omega)}{\omega^2+\zeta^2} d\omega = \frac{2\omega_p^2\omega_\tau}{\pi(\zeta^2 - \omega_\tau^2)}\left[\frac{\arctan(\omega_1/\omega_\tau)}{\omega_\tau} - \frac{\arctan(\omega_1/\zeta)}{\zeta}\right]. \tag{8}$$

The dielectric functions at imaginary frequencies $\varepsilon(i\zeta)$, calculated via equation (6) for the various materials in figure 1(*a*), are shown in figure 1(*b*). The distinct optical responses of Au, AIST, and SiC are clearly visible at real frequencies. Figure 1(*b*) shows that this difference occurs at imaginary frequencies too. Moreover, the difference is significant in the range $0.1 < \zeta < 1$ eV that gives the most important contribution to the Casimir force at distances $z \sim 100$ nm [8, 9, 11, 12, 16].

Finally, in order to illustrate the strong material influence on the Casimir force for the systems studied here (figure 1), we introduce the reduction factor $\eta_{sp}(z)$ ($\leqslant 1$) to normalize the Casimir force with respect to the maximum possible force between ideal metals [2]

$$\eta_{sp}(z) = \frac{F^{ps}(z)}{F^{ps}_{ideal}(z)}, \qquad F^{ps}_{ideal}(z) = \frac{\pi^3 R\hbar c}{360\, z^3}. \tag{9}$$

The reduction factors $\eta_{sp}(z)$ calculated for different materials are shown in figure 2. They indicate the distinct nature of the different systems. Within the maximum distance for our actuation studies ($\sim$200 nm), for the Au–SiC system $\eta_{sp,\ Au-SiC}(z) \sim 0.3$ while for the Au–Au system this factor is almost doubled to $\eta_{sp,\ Au-Au}(z) \sim 0.6$. The materials' influence is reduced at shorter separations ($<$10 nm), where more detailed information on $\varepsilon''(\omega)$ at higher frequencies ($>\omega_2$) is needed for accurate Casimir force calculations [8, 9, 11, 12, 16]. The significant differences among the Casimir forces for the investigated materials have to affect the actuation dynamics of MEMS considerably.

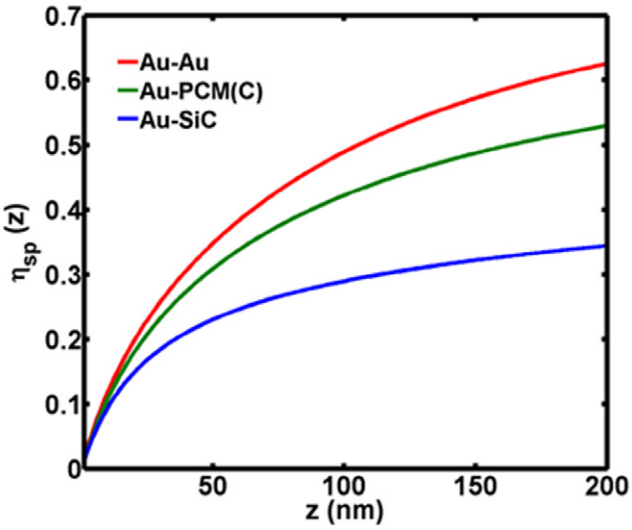

Figure 2. Casimir reduction factor for different pairs of materials: Au–Au, Au–PCM (C), and Au–SiC. As a PCM system we used the optical data of crystalline (C) AIST [8, 9] (figure 1).

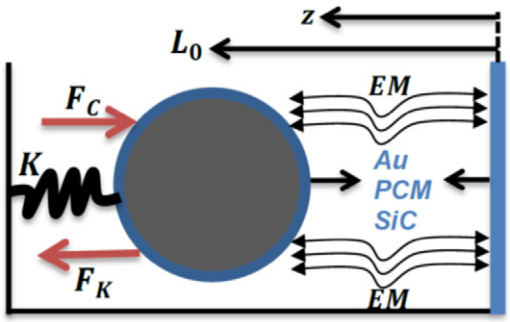

Figure 3. Conceptual schematic of an actuated MEM system with the corresponding acting forces.

3. Materials' influence on MEMS actuation

Next, we model the actuation dynamics of a simplified MEMS device (in the form of a microswitch). To this end, we consider a moving sphere interacting with a fixed plate, where both components are assumed to be coated with a thick ($\geqslant$100 nm) coating of SiC, AIST or Au (figure 3). In this geometry, typically used for force measurements [8–12], the Casimir force $F^{ps}(z)$ is opposed by the elastic restoring force $F_K(z) = -K(L_0 - z)$, where K is the spring constant. It should be kept in mind that the calculation of the Casimir force by pairwise summation (i.e., the assumption that different contributions to the Casmir force are independent of each other) is not, in general, a good approximation for arbitrary MEMS geometries. Note that because the Casimir force is proportional to the sphere's radius R in equation (1), the larger the R (or more generally, the size of the actuating component), the larger the values of K that are required for stable actuation.

We assume that an initial impulse (e.g., an electrical signal) triggers continuous actuation, where L_0 ($=200$ nm) denotes the separation where the spring is not stretched. Then the equation of motion has the form [16–18, 21]

$$M\frac{\mathrm{d}^2z}{\mathrm{d}t^2}+\left(\frac{M\omega}{Q}\right)\left(\frac{\mathrm{d}z}{\mathrm{d}t}\right)=-K(L_0-z)+F^{\mathrm{ps}}(z). \qquad (10)$$

Here M is the mass of the sphere, and $(M\omega/Q)$ $(\mathrm{d}z/\mathrm{d}t)$ is intrinsic energy dissipation in the actuating system. Initially we consider MEMS with a high quality factor $Q \geqslant 10^4$ [22] so that we can neglect dissipation effects. The frequency ω is assumed to be that of dynamic mode atomic force microscope (AFM) cantilevers or MEMS (typically $\omega = 300$ kHz) [22]. In each case we will assume the surfaces are flat, because nanoscale roughness gives significant contributions only at separations below 100 nm [8, 16].

To characterize the stability problem let us introduce the parameter $\lambda \equiv F^{\mathrm{ps}}(L_0)/KL_0$, which is the ratio of the minimum Casimir force $F^{\mathrm{ps}}(L_0)$ to the maximum elastic force KL_0. The parameter λ plays the role of a bifurcation parameter: a small change in λ can lead to a sudden qualitative change in the actuation of MEMS. Our purpose is to compare the actuation in the presence of the Casimir force for devices made from different materials. Equilibrium points of equation (10) correspond to the total force being equal to zero: $F_{\mathrm{tot}} = -K(L_0 - z^*) + F^{\mathrm{ps}}(z^*) = 0$. From this condition the locus of the equilibrium points z^* can be obtained [16–18, 21]. Thus we obtain for λ the following expression

$$\lambda = \left(F^{\mathrm{ps}}(L_0)/F^{\mathrm{ps}}(z^*)\right)\left(1 - z^*/L_0\right). \qquad (11)$$

The right hand side of this equation defines the function $f(z^*)$, which is going to zero at $z^* \to 0$ and $z^* \to L_0$, and has a maximum in between these points. There are no steady-state solutions if $\lambda > f_{\max}$ where $f_{\max} = f\left(z^*_{\max}\right)$ with $z^*_{\max}$ corresponding to the maximum of the λ versus z^* plots in figure 4. In this case the Casimir force dominates and the components inevitably stick to each other.

Figure 4 illustrates the situation with respect to the stability of the system. If the spring constant is strong enough so that $\lambda < f_{\max}$ then there are two equilibria. The stationary points closest to L_0 are stable centers around which periodic solutions exist (indicated by the circles for example for Au–Au and SiC–SiC in figure 4), whereas the ones closer to the plate are unstable saddle points. Motion around these points will lead to stiction onto the plate due to the stronger Casimir force. The equilibrium points $z^* > z^*_{\max}$ correspond to stable actuation. For a sufficiently small spring constant K so that $\lambda > f_{\max}$, for example for the Au–Au interaction, the motion is unstable and favors stiction, while there can still be two equilibrium points for the SiC–SiC system. Clearly the SiC–SiC system has a much wider range of stable operation than that of Au–Au. All possible bifurcation curves for the different materials under investigation here are included in between the ones of the SiC–SiC and the Au–Au systems, as shown in figure 4.

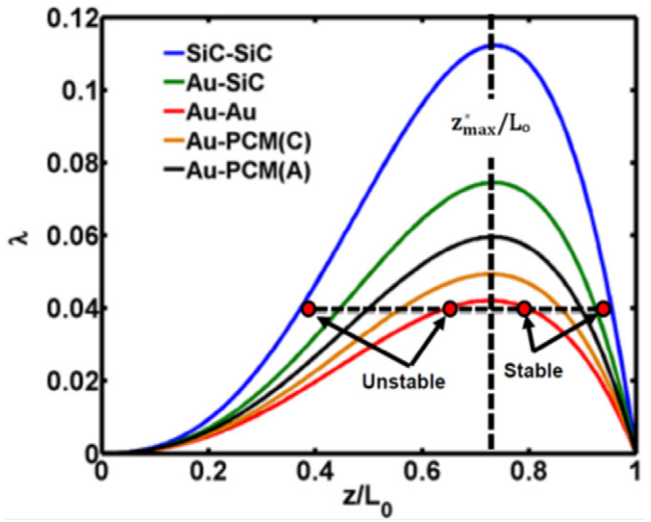

Figure 4. Bifurcation diagrams for all material combinations Au, SiC, and PCMs using the Drude model for the Casimir force calculations. The position of the maximum is indicated for illustration purposes only for the Au–Au system.

Furthermore, the system dynamics via the solution of the equation of motion can be described with the so-called phase portraits [19], which are plots of the velocity $\mathrm{d}z/\mathrm{d}t$ of the actuating element versus its displacement z. Phase portraits for different samples of materials are presented in figure 5(a) for all materials presented in figure 1. Closed orbits correspond to periodic motion around a stable center equilibrium point. This indicates that the elastic force is strong enough to counterbalance the Casimir force. Figure 5(b) shows phase portraits for different gold films characterized optically in [11]. These films have different plasma frequencies ω_{p} and relaxation times ω_τ for samples 1, 3, and 5, respectively [11]. From this figure it becomes clear that by changing material preparation conditions, the domain of system movement and thus its stability can be influenced significantly. The difference between films notably increases for the part of the orbit that comes close to the plate, since that is where the Casimir force is strongest. In addition, figure 6 shows more details of how a system can transit progressively from stable motion into stiction by changing the material optical properties. The Au–Au system that has the strongest Casimir attraction moves the actuating sphere rapidly into stiction, while for the other materials periodic motion is still feasible. If we compare Au and SiC, then the actuating component coated with the latter remains safely far from the unstable saddle and the system experiences only stable movement.

Finally, we point out that although the stronger Casimir force predicts stiction under conditions of low dissipation ($Q \gg 1$, figure 6), the introduction of dissipation (by decreasing the value of Q) can strongly alter the nature of the instability as figure 7 indicates for Au. Indeed, as the system quality factor Q drops by an order of magnitude, then stiction instability turns into the more stable dissipative motion towards a stable sink equilibrium since the work performed on the actuating component by the Casimir force can no longer overcome dissipative losses.

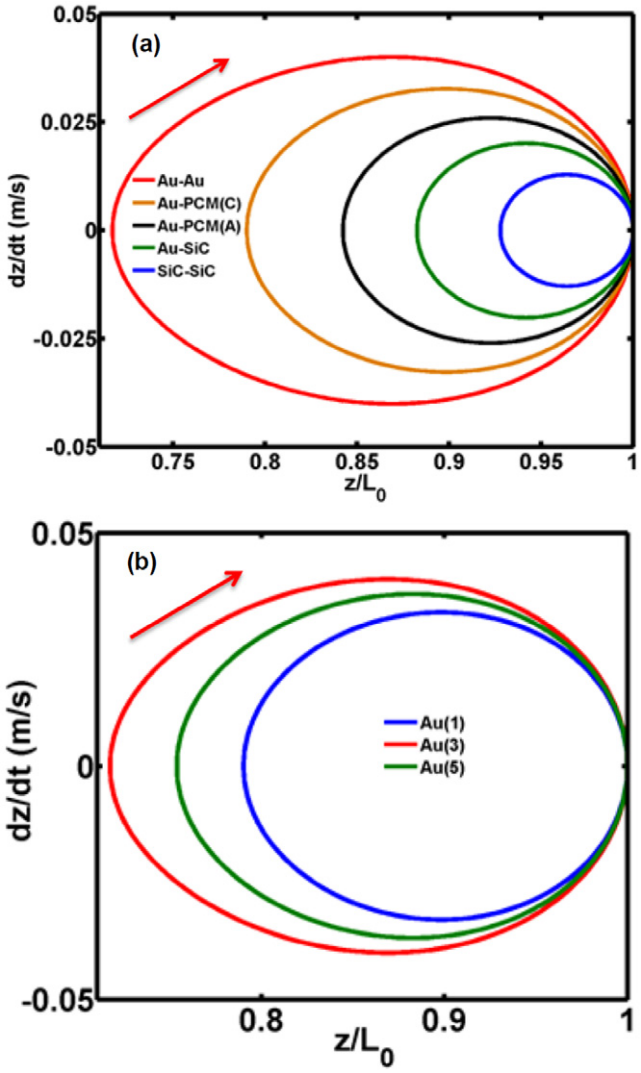

Figure 5. (*a*) Phase portraits for Au, SiC and PCM (C) systems using the Drude model. (*b*) Phase portraits when the plate is coated with three different Au films from [11] using the Drude model. The spring constant was in all cases $K = 0.000\,15\,\mathrm{N\,m^{-1}}$, and $R = 10\,\mu\mathrm{m}$. The arrow indicates the direction of motion.

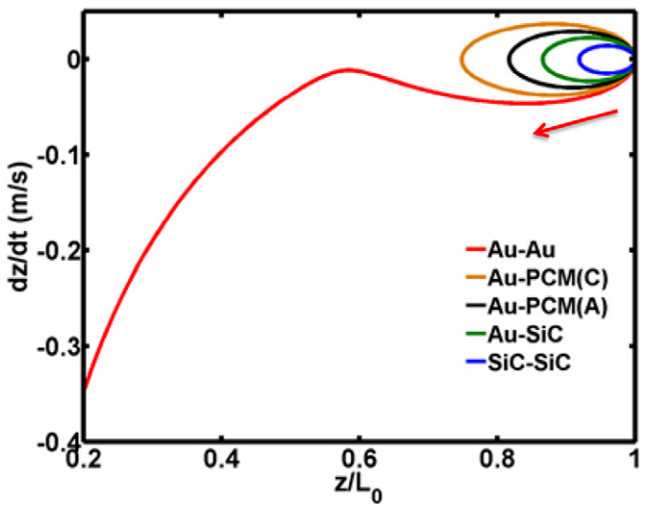

Figure 6. Phase portrait $\mathrm{d}z/\mathrm{d}t$ versus z for different materials for the sphere and plate. Closed orbits show stable motion, while an open orbit is the sign of unstable motion towards stiction onto the plate. The spring constant is $K = 0.000\,10\,\mathrm{N\,m^{-1}}$, and $R = 10\,\mu\mathrm{m}$. The arrow indicates the direction of motion.

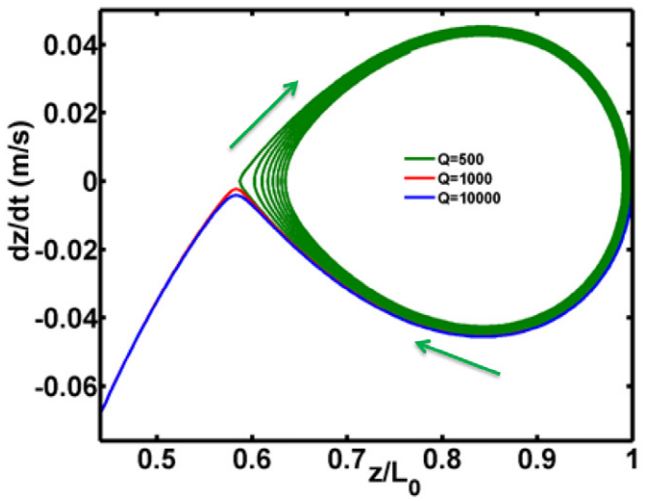

Figure 7. Influence of dissipation with different Q factors on actuation dynamics of a MEMS using the Drude model for Au. The spring constant was $K = 0.000\,10\,\mathrm{N\,m^{-1}}$, and $R = 10\,\mu\mathrm{m}$. The arrows indicate the direction of motion.

4. Conclusions

In conclusion, the dependence of the Casimir force on the frequency-dependent dielectric function of interacting materials makes it feasible to tailor the actuation dynamics of microactuators. Furthermore, bifurcation analysis with phase portraits was used to compare the sensitivity of model actuators when the optical properties are changing by taking into account different dissipation at low optical frequencies. The Casimir force is largest for metal–metal interacting systems due to the high absorption of conduction electrons in the infrared range, whereas for less conductive systems such as the PCMs and SiC the Casimir forces are weaker. This makes device actuation more stable at shorter separations against pull-in instabilities that lead to stiction. Finally, our analysis indicates that the stronger Casimir force can lead to stiction, while decreasing the system Q factor increases the range of conditions under which the actuation is stable.

Acknowledgments

We would like to acknowledge support from the Zernike Institute of Advanced Materials, University of Groningen, The Netherlands.

References

[1] Rodriguez A W, Capasso F and Johnson S G 2011 *Nat. Photonics* **5** 211
Ball P 2007 *Nature* **447** 772
[2] Casimir H B G 1948 *Proc. K. Ned. Akad. Wet.* **51** 793
[3] Lifshitz E M 1956 *Sov. Phys. JETP* **2** 73
Dzyaloshinskii I E, Lifshitz E M and Pitaevskii L P 1961 *Sov. Phys. Usp.* **4** 153
[4] Lamoreaux S K 1997 *Phys. Rev. Lett.* **78** 5
Lamoreaux S K 2005 *Rep. Prog. Phys.* **68** 201
Chan H B *et al* 2001 *Phys. Rev. Lett.* **87** 211801

Chan H B *et al* 2001 *Science* **291** 1941
Decca R S *et al* 2005 *Ann. Phys.* **318** 37
Decca R S *et al* 2007 *Phys. Rev.* D **75** 077101
[5] Iannuzzi D, Lisanti M and Capasso F 2004 *Proc. Natl Acad. Sci. USA* **101** 4019
[6] Chen F, Klimchitskaya G L, Mostepanenko V M and Mohideen U 2007 *Opt. Express* **15** 4823
Torricelli G, Pirozhenko I, Thornton S, Lambrecht A and Binns C 2011 *Europhys. Lett.* **93** 51
[7] de Man S, Heeck K, Wijngaarden R J and Iannuzzi D 2009 *Phys. Rev. Lett.* **103** 040402
[8] Torricelli G, van Zwol P J, Shpak O, Binns C, Palasantzas G, Kooi B J, Svetovoy V B and Wuttig M 2010 *Phys. Rev.* A **82** 010101 (R)
[9] Torricelli G, van Zwol P J, Shpak O, Palasantzas G, Svetovoy V B, Binns C, Kooi B J, Jost P and Wuttig M 2012 *Adv. Funct. Mater.* **22** 3729
[10] Chang C-C, Banishev A A, Klimchitskaya G L, Mostepanenko V M and Mohideen U 2011 *Phys. Rev. Lett.* **107** 090403
[11] Svetovoy V B, van Zwol P J, Palasantzas G and DeHosson J Th M 2008 *Phys. Rev.* B **77** 035439
[12] Palasantzas G, Svetovoy V B and van Zwol P J 2010 *Int. J. Mod. Phys.* B **24** 6013
[13] Decca R S, López D, Fischbach E, Klimchitskaya G L, Krause D E and Mostepanenko V M 2007 *Phys. Rev.* D **75** 077101
Chang C-C, Banishev A A, Castillo-Garza R, Klimchitskaya G L, Mostepanenko V M and Mohideen U 2012 *Phys. Rev.* B **85** 165443
[14] Behunin R O *et al* arXiv:1407.3741
For patch effects see also: Behunin R O *et al* 2012 *Phys. Rev.* A **85** 012504
Behunin R O *et al* 2012 *Phys. Rev.* A **86** 052509
[15] Wuttig M and Yamada N 2007 *Nat. Mater.* **6** 824
[16] Sedighi M, Svetovoy V B, Broer W H and Palasantzas G 2014 *Phys. Rev.* B **89** 195440
[17] Sedighi M, Broer W H, Palasantzas G and Kooi B J 2013 *Phys. Rev.* B **88** 165423
[18] Sedighi M and Palasantzas G 2014 *Appl. Phys. Lett.* **104** 074108
[19] Cheung R 2006 Silicon carbide MEMS for harsh environments *Introduction To Silicon Carbide (SiC) Microelectromechanical Systems (MEMS)* ed R Cheung (Edinburgh: University of Edinburgh) chapter 1
Sarro P M 2000 *Sensors Actuators* **82** 210
[20] Stark B 1999 *MEMS Reliability Assurance Guidelines for Space Applications* JPL Publication 99-1 (Pasadena, CA: California Institute of Technology)
[21] Esquivel-Sirvent R, Reyes L and Bárcenas J 2006 *New J. Phys.* **8** 241
Esquivel-Sirvent R, Palomino-Ovando M A and Cocoletzi G H 2009 *Appl. Phys. Lett.* **95** 051909
[22] Garcıa R and Perez R 2002 *Surf. Sci. Rep.* **47** 197
Li M, Tang H X and Roukes M L 2007 *Nat. Nanotechnol.* **2** 114
Mamin H J and Rugar D 2011 *Appl. Phys. Lett.* **79** 3358
Rugar D, Budakian R, Mamin H J and Chui B W 2004 *Nature* **430** 329